

# Coherent optical receiver for PPM signals received through atmospheric turbulence: Performance analysis and preliminary experimental results

<sup>1</sup>M. Muñoz Fernández\*, V. A. Vilnrotter  
Jet Propulsion Laboratory, California Institute of Technology

## ABSTRACT

The performance of a coherent free-space optical communications system is investigated. Bit Error Rate (BER) performance is analyzed, and laboratory equipment and experimental setup used to carry out these experiments at the Jet Propulsion Laboratory are described. The key components include two lasers operating at 1064 nm wavelength for use with coherent detection, a 16 element (4X4) focal plane detector array, and data acquisition and signal processing assembly needed to sample and collect the data and analyze the results. Combining of the signals out of phase from the focal plane is accomplished using the least-mean-square algorithm (LMS).

**Keywords:** Coherent optical communications, Pulse Position Modulation, focal plane array.

## 1. INTRODUCTION

Optical space communications systems are becoming more practical as technology develops and offer significant advantages over radio frequency communications. The main advantages are the ability to concentrate power in extremely narrow beams, the potential increase in modulation bandwidth and the drastic reduction in component sizes. Optical wavelengths are very short, and correspond to very high carrier frequencies. Increasing the carrier frequency theoretically increases the available transmission bandwidth, and therefore the information capacity of the system. As a result, frequencies in the optical range may have potential bandwidths of approximately  $10^5$  times that of a carrier in the RF range [1].

Intensity modulation with direct detection is currently used for optical communications systems. Under ideal transmission and detection conditions, the probability of detecting  $n$  photons in a pulse train having an average of  $N_p$  photons per pulse obeys the Poisson

distribution [1,2] 
$$p(n) = \frac{N_p^n e^{-N_p}}{n!} \quad (1)$$

The probability of an erasure is defined as the detection of no photons during the pulse, and given by 
$$P_E = \exp(-N_p) \quad (2)$$

For example, an average of 21 detected photons per pulse would be needed to achieve an erasure probability of  $10^{-9}$ . This limit is rarely reached since it assumes no dark or background counts whatsoever in the receiver. In the presence of background radiation, performance of direct detection receivers degrades significantly, as shown in [2]. One way to overcome the effects of background radiation is to use coherent detection. With coherent detection, a beam of light (the local oscillator) mixes with the modulated wave at the photodetector as shown in Fig. 1 [3].

---

<sup>1</sup>The research described in this publication was carried out by the Jet Propulsion Laboratory, California Institute of Technology, under a contract with the National Aeronautics and Space Administration.

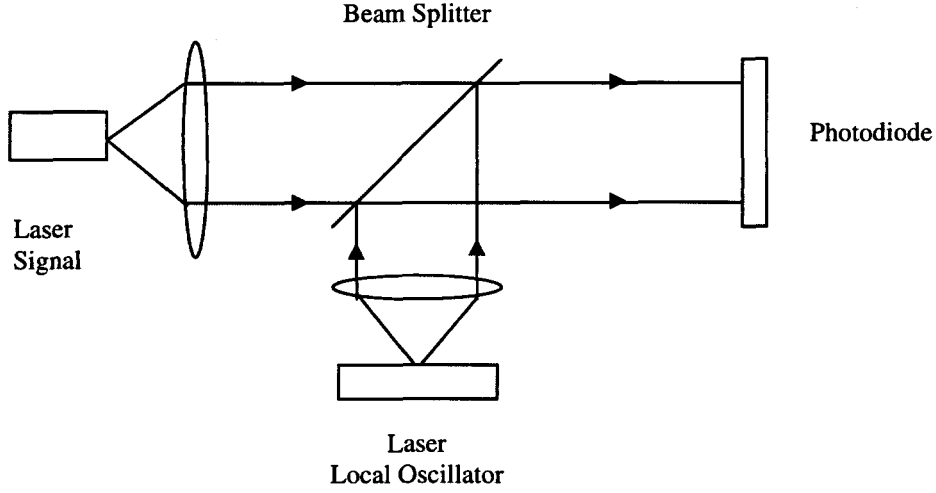


Figure 1. Combining of the transmitted signal and local oscillator beams

If the LO is the same wavelength as the received optical signal, and in addition is in phase with the optical carrier, the detection is called homodyne detection. If the frequencies of the LO and received signal are different, then it is called heterodyne detection. The heterodyne detector converts phase changes in the optical carrier to phase changes in the optical intensity, which are reproduced in the detected current waveform. The following analysis shows how the heterodyne scheme permits detection of the incoming signal beam. If beams are spatially well aligned, there is optical interference on the photodetector surface, resulting in the intensity

$$I \propto (E_s + E_L)^2 \quad (3)$$

This inherent squaring operation of the photodetector produces a detector current at the intermediate frequency which contains the signal modulation. If the carrier and local oscillator beams are aligned perpendicular to the photodetector surface, the expression of the field incident on the detector is:

$$E(t) = E_s(t) \cos[\omega_s t + \phi_s] + E_L(t) \cos[\omega_L t + \phi_L] \quad (4)$$

The photodetector output current is proportional to the detector responsivity and the optical intensity. The responsivity is given by

$$\mathfrak{R} = \frac{e\eta_q}{h\nu} [\text{amps/Watt}] \quad (5)$$

where  $e$  is the electronic charge,  $\eta_q$  is the detector quantum efficiency,  $h$  is Planck's constant and  $\nu = \omega / 2\pi$  is the optical frequency. Therefore,

$$i(t) = \frac{e\eta_q}{2h\nu} [E(t)]^2 \quad (6)$$

$$E^2(t) = [E_s(t) \cos(\omega_s t + \phi_s) + E_L(t) \cos(\omega_L t + \phi_L)]^2 \quad (7)$$

High frequency intensity components that oscillate near twice the optical carrier frequency are eliminated from the receiver as that frequency is much greater than the frequency response of the detector [4]. Therefore, we can write the intensity as:

$$I(t) = E^2(t) = \frac{1}{2} E_L^2(t) + \frac{1}{2} E_s^2(t) + E_L(t) E_s(t) \cos[(\omega_L - \omega_s)t + \phi_L - \phi_s] \quad (8)$$

Detected current is proportional to the average optical intensity, where the average is taken over a time interval long compared to the optical period, but short compared to the period of the IF.

$$i(t) = i_L(t) + i_s(t) + 2\sqrt{i_L(t)i_s(t)} \cos[(\omega_L - \omega_s)t + \phi_L - \phi_s] \quad (9)$$

Where  $i_L = \Re E_L^2/2$  and  $i_s = \Re E_s^2/2$  are the dc contributions from the local oscillator and signal beams. Expressing in terms of the signal fields:

$$i(t) \propto E^2(t) = E_L^2(t) + E_s^2(t) + 2E_L(t)E_s(t) \cos[(\omega_L - \omega_s)t + \phi_L - \phi_s] \quad (10)$$

If the local oscillator power is much greater than the signal power, the second term of Eq. (10) can be neglected. The first term represents a large and continuous signal that carries no information but generates a shot noise contribution. The third term represents the signal modulation. If the signal is coupled to a detector of responsivity  $\Re$  and ac-coupled to eliminate the local oscillator signal,

$$i(t) \propto E^2(t) \cong 2E_L(t)E_s(t) \cos[(\omega_L - \omega_s)t + \phi_L - \phi_s] \quad (11)$$

The two sources may oscillate at nominally different frequencies, the difference being labeled the intermediate frequency. If this intermediate frequency is zero, the detection process is termed homodyne detection. When there is a difference frequency for postdetection processing, it is called heterodyne detection.

In coherent communications the optical frequency and the phase of the signal relative to those of the local oscillator are preserved, including the phase and frequency fluctuations whenever the oscillator has enough stability. The local oscillator preamplifies the signal, improving the signal-to-noise ratio in the limit of local oscillator power. For the shot-noise limited case, when effects of dark current and thermal noise are eliminated by raising the optic power and with  $e=1$ , the resulting signal-to-noise ratio for heterodyne detection is:

$$\frac{S}{N} = \frac{\eta_q P_s}{h\nu\Delta\nu} \quad (12)$$

Therefore, the minimum detectable signal (signal input power leading to an output signal-to-noise ratio of 1) is [5]:

$$(P_s)_{\min} = \frac{h\nu\Delta\nu}{\eta_q} \quad (13)$$

In the case of homodyne detection, the signal-to-noise ratio is:

$$\frac{S}{N} = 2 \frac{\eta_q P_s}{h\nu\Delta\nu} \quad (14)$$

In the case of direct detection [6],

$$\frac{S}{N} = \frac{1}{2} \frac{\eta_q P_s}{h\nu\Delta\nu} \quad (15)$$

The shot-noise limited SNR obtained in homodyne detection is a factor of two better than the heterodyne receiver and a factor of four (6dB) better than the SNR of a direct detection system.

The case of heterodyne optical detection is studied in this case as quantum-limited performance can theoretically be obtained and receiver sensitivities of the order of 10-20 dB higher than direct detection systems are possible under high background conditions [7].

## 2. PERFORMANCE ANALYSIS OF A COHERENT OPTICAL RECEIVER FOR M-ARY PPM SIGNALS

When heterodyne detection is used, digital bits could also be encoded directly on the phase or frequency of the laser carrier itself. The received modulated laser carrier can be translated to a lower RF frequency, where the digital modulation can be decoded using standard RF decoding techniques [8].

Pulse Position Modulation (PPM) is used in the heterodyne detection system proposed. PPM is a form of block encoding in which bits are transmitted in blocks instead of one at a time [8]. Optical block encoding is achieved by converting each block of  $b$  bits into one of  $M=2^k$  optical fields of transmission. At the receiver end, decoding of each block is performed by determining which one of the  $M$  fields is received per block time. For the PPM case, a PPM frame contains  $M$  slots and an optical pulse is placed in one of those  $M$  slots. The data word is determined based on the position of the optical pulse in the frame. The PPM format is shown in Figure 2.

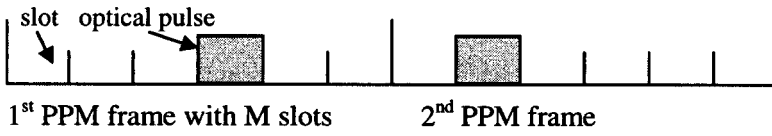


Figure 2. Pulse Position Modulation format.

The receiver decides on the basis of a maximum likelihood symbol detection probability; it selects the slot with the greatest voltage and the symbol that contains a signal pulse in that slot location is the transmitted symbol.

If  $A$  is the aperture area of the detector,  $\alpha = \eta q / h\nu$ , and  $E_L \gg E_s$ , the time average of the statistical average of the resulting intensity counting rate process ( $i(t)$ ) of the photodetector,  $\bar{i}$  from (Eq.11) is [1]:

$$\begin{aligned} \bar{i} &= \alpha A |a(t)|^2 = \alpha A E_L^2 + \alpha A 2 E_s E_L \cos[(\omega_L - \omega_s)t + \phi_L - \phi_s] \\ &= i_L + i_s(t; (\omega_L - \omega_s), \phi_L, \phi_s) \end{aligned} \quad (16)$$

The local power alone sets the shot noise level of spectral level  $N_s/2$ . In case of perfect phase tracking,  $\phi_L - \phi_s = 0$ , and if homodyne detection,  $\omega_L - \omega_s = 0$ .

Under shot-noise limited conditions, the received optical signal at the detector is:

$$r(t) = i(t) + n(t) \quad (17)$$

Where  $n(t)$  is a Gaussian noise voltage of spectral level  $N_s / 2 = \alpha A E_L^2$

The variance of the shot-noise voltage is calculated integrating for  $\tau$  seconds (duration of the PPM pulse in the  $i$ th slot) resulting  $\sigma_s^2 = \alpha A E_L^2 \tau$

The value of the signal voltage for homodyne detection is obtained integrating as well for  $\tau$  seconds for a signal slot is:

$$v_d = 2 E_s E_L \alpha A \tau \quad (18)$$

The signal-to-noise ratio is therefore:

$$SNR = \frac{P_{signal}}{P_{noise}} = \frac{[2 E_s E_L \alpha A \tau]^2}{\alpha A E_L^2 \tau} = 4 \alpha A E_L^2 \tau = 4 K_s \quad (19)$$

where  $K_s = \alpha A E_L^2 \tau$  is the average number of signal photons that would be detected over the same time interval (by direct detection).

For the case of heterodyne detection and following the previous equations, the only difference is that now  $(\omega_L - \omega_s) \neq 0$  and the values obtained are as follows:

$$\bar{i} = \alpha A |a(t)|^2 = \alpha A E_L^2 + \alpha A 2 E_s E_L \cos[(\omega_L - \omega_s)t] = i_L + i_s(t) \quad (20)$$

$$v_d = v_{rms} = \frac{2}{\sqrt{2}} E_s E_L \alpha A \tau = \sqrt{2} E_s E_L \alpha A \tau \quad (21)$$

$$SNR = \frac{P_{signal}}{P_{noise}} = \frac{[\sqrt{2} E_s E_L \alpha A \tau]^2}{\alpha A E_L^2 \tau} = 2 \alpha A E_L^2 \tau = 2 K_s \quad (22)$$

A high count rate at the detector output is assumed due to the local field condition, which determines the Gaussian nature of shot noise. Therefore, heterodyne detector outputs are assumed as Gaussian processes in most cases with the signal term corresponding to the modulated carrier, and all other spectral components considered as additive Gaussian noise with the spectra given [1]. The resulting SNR could be taken as coming from a constant signal of voltage value  $v_d = \sqrt{SNR}$ , observed in the presence of noise voltage with zero mean and variance equal to 1. As the photodetected mixed field can be modeled as a Gaussian process, the

probability density of this signal would be 
$$P_{SIGNAL\ SLOT}(x) = \frac{1}{\sqrt{2\pi}} e^{-(x-\sqrt{SNR})^2/2} \quad (23)$$

And for the remaining slots with no signal, the process could be modeled as a Gaussian random variable with zero mean and unit variance 
$$P_{SLOT\ NO\ SIGNAL}(x) = \frac{1}{\sqrt{2\pi}} e^{-x^2/2} \quad (24)$$

These expressions are accurate under strong local field condition and weak background radiation [1]. Since PPM signals are a type of orthogonal signals, for the homodyne detection case, the probability of correct symbol could be expressed as [10], [11]:

$$P(SC) = \int_{-\infty}^{+\infty} \frac{1}{\sqrt{2\pi}} e^{-(x-\sqrt{4K_s})^2/2} dx \left[ \int_{-\infty}^x \frac{1}{\sqrt{2\pi}} e^{-y^2/2} dy \right]^{M-1} \quad (25)$$

If equal a-priori transmission probabilities are assumed for each symbol, the probability of symbol error can be expressed as:  $P(SE) = 1 - P(SC)$

Finally to obtain the bit error probability for homodyne detection as  $P_e = [(M/2)/(M-1)]P(SE)$  [1]:

$$P_e = \frac{M/2}{M-1} \left[ 1 - \left\{ \int_{-\infty}^{+\infty} \frac{1}{\sqrt{2\pi}} e^{-(x-\sqrt{4K_s})^2/2} dx [1 - Q(x)]^{M-1} \right\} \right] \quad (26)$$

$$P_e = \frac{M/2}{M-1} \left[ 1 - \left\{ \int_{-\infty}^{+\infty} \frac{1}{\sqrt{2\pi}} e^{-(x-\sqrt{4K_s})^2/2} dx \left[ \frac{1}{2} - \frac{1}{2} \operatorname{erf} \left( \frac{x}{\sqrt{2}} \right) \right]^{M-1} \right\} \right] \quad (27)$$

And for heterodyne detection could be expressed as:

$$P_e = \frac{M/2}{M-1} \left[ 1 - \left\{ \int_{-\infty}^{+\infty} \frac{1}{\sqrt{2\pi}} e^{-(x-\sqrt{2K_s})^2/2} dx \left[ \frac{1}{2} - \frac{1}{2} \operatorname{erf} \left( \frac{x}{\sqrt{2}} \right) \right]^{M-1} \right\} \right] \quad (28)$$

The union bound for the case of homodyne detection can be derived following [10] and the bit error probability can be approximated as

$$P_e \cong \left( \frac{M}{2} \right) \left[ Q[\sqrt{2K_s}] \right] = \left( \frac{M}{2} \right) \left\{ \frac{1}{2} \operatorname{erfc} [\sqrt{K_s}] \right\} \quad (29)$$

The bit error probability for heterodyne detection approximated with the union bound would be

$$P_e \cong \left(\frac{M}{2}\right) \left[ Q\left(\sqrt{K_s}\right) \right] = \left(\frac{M}{2}\right) \left\{ \frac{1}{2} \operatorname{erfc} \left[ \sqrt{\frac{K_s}{2}} \right] \right\} \quad (30)$$

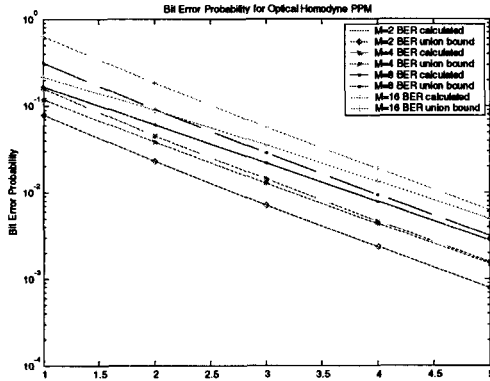


Figure 3.1. BER for optical homodyne detection

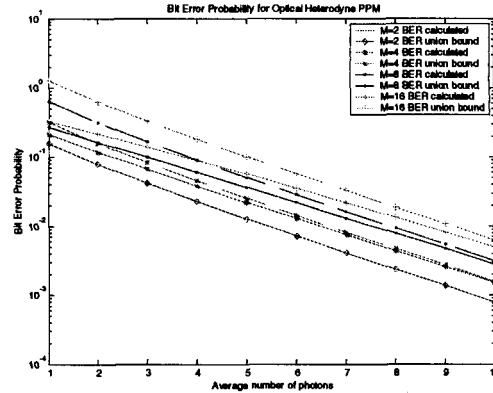


Figure 3.2. BER for optical heterodyne detection

## 2. EXPERIMENTAL RESULTS AND ANALYSIS

The experimental setup of the optical coherent combining experiment consists of two Nd:YAG lasers operating at 1064 nanometers, whose outputs are aligned and combined on the surface of a 4X4 Fermionics InGaAs detector array. One of the lasers serves as a local oscillator (high output power, 50 mW), while the other simulates the received signal (2-3 mW output). The two lasers are operated at slightly different wavelengths, yielding a relatively stable difference-frequency tone of approximately 6 MHz in the detected signal. The difference-frequency tone is generally observable in several array elements simultaneously, but usually with different phases. If the detector element outputs were simply summed, the addition of out-of-phase tones could result in significant cancellation, yielding a weak signal tone at the output. Non-coherent addition of signal components from different elements of the detector array is analogous to detection with a single large detector: this is the prime reason why a single large detector is not effective for coherent detection of signal fields under turbulent conditions. However, if small areas of the detector surface over which the signal field is essentially coherent are processed separately, then the outputs can be phase-aligned prior to addition, recovering the lost signal power.

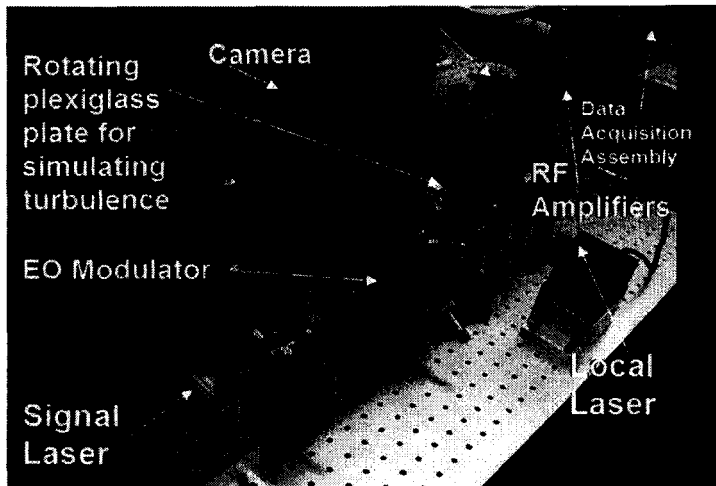
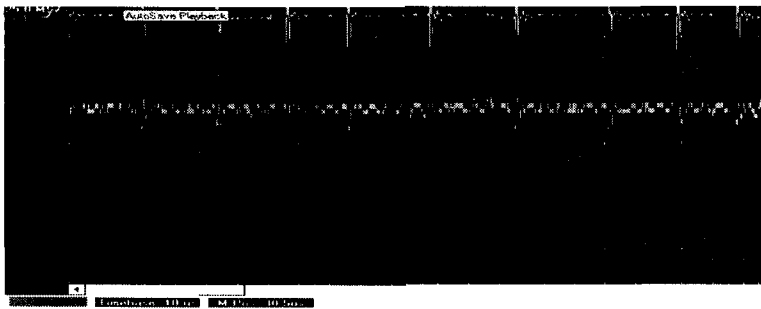


Figure 4. Coherent combining experiment at the Jet Propulsion Laboratory, NASA.

In the current coherent combining experiment, each of the 16 outputs of the detector array are amplified, and input to a 16-channel data-acquisition assembly (the data-acquisition is currently carried out using GaGe cards). The analog signals are digitized to 8 bits at a sampling rate of 25 mega-samples per second (MSPS). The data-acquisition system is capable of synchronously “grabbing” up to 1 megabyte of data per channel (or one million 8-bit samples), however we have elected to work with only 104128 samples per channel for these tests, in order to simplify the data-transfer from the data-acquisition computer to the signal-processing computer. At a sampling rate of 25 MSPS, this sample-stream represents 4.16512 ms of elapsed time. We have identified four channels that contained significant signal, and at a certain time synchronously collected 104128 samples from each channel (in a realistic communications scenario, the combining algorithm would automatically select the “signal” pixels for processing).The modulation format for the transmitted laser signal is PPM using an external Electro-Optic Modulator (Pockle cell). At the GaGe scope we can see the PPM modulated beatnotes (Fig. 5) at a rate of 97.65 kHz. The PPM frame period is exactly 10.24  $\mu$ s. The slot width is approximately 300ns, obtaining approximately a 32-PPM system.



**Figure 5.** PPM Beatnotes observed the the GaGe Scope data acquisition assembly

The nominally 6 MHz signal-tones were downconverted to complex baseband, and input to the least-mean-square algorithm, or LMS, currently under development. This adaptive algorithm automatically estimates the complex weights required to reconstruct the signal, then it applies the weights to the complex signal in each channel, and combines the “phased-up” signals in order to maximize power, or SNR. A rotating pre-distorted plexiglass plate was incorporated to simulate atmospheric turbulence. Intensity distributions of signal beam at the input to the focal-plane array with and without simulated turbulence are shown in Fig. 6.

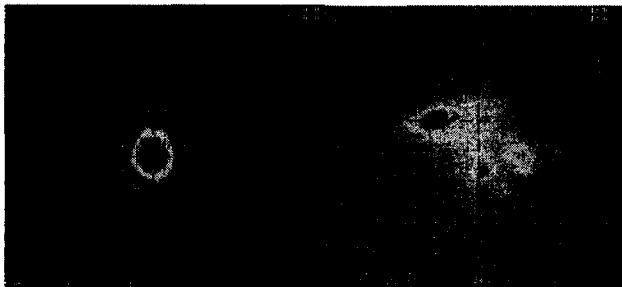


**Figure 6.** Beam profile without and with atmospheric turbulence from left to right

### The LMS Algorithm

The discrete complex version of the LMS algorithm can be described by the following recursive equation as described in references [13], [14]:

$$\omega_p(n+1) = \omega_i(n) + \mu \tilde{x}_i^*(n) \tilde{E}(n) \quad (31)$$

The LMS algorithm is a recursive equation that allows the value of each weight  $\omega_p$  at the (n+1) sample to be calculated from its value at the nth sample, using the signals at the nth sample. The

sampled error signal in Eq. (32) is obtained from the sampled reference signal and array output, is as follows:

$$\varepsilon(n) = r(n) - s(n) = r(n) - \sum_{j=1}^N \omega_{p_j}(n) x_{p_j}(n) \quad (32)$$

In our case, the reference signal that we use is a constant value calculated based on the addition of the magnitude of the signal in the four channels, of value 0.06 (Fig. 13) in our case. Therefore, the error signal obtained is a complex number that contains the phase information required. The error signal has to be minimized in order for the phase weights to converge; at that point, the four signals will be phased up for perfect combining and therefore the combined output is maximized. The weights transients are computed from Eq. (31) starting with zero initial values. Depending on the  $\mu$ , called “step-size”, the slope of the combining output changes as it is higher for greater values of the step-size. Varying  $\mu$ , it is possible to control what fraction of the latest weight-estimate is applied to the current weight during each update, providing additional smoothing to the weight estimates. Small step-size tends to produce good weight estimates under static conditions, however generally leads to greater “weight misadjustment” under dynamic conditions (such as severe Doppler, or severe differential drift between local and signal wavelengths) as the weight estimates cannot keep up with the dynamics. Therefore, there is typically a best step-size to use for each situation. After some experimentation, we have determined that for this data-set good results could be obtained by correlating over 10,000 samples, and using a step-size of 1,000. We can see that after approximately 30 samples, the weights converge as we obtain the maximum combined power and minimum error; that translates in 1.2 $\mu$ s of acquisition region.

Referring to Figs. 7, 8, and 9 with  $\mu=10$ , we see that when the step-size is so small that the LMS algorithm cannot keep up with the phase variations in the beatnote, the combining output signal shows that the four channels are not perfectly combined as it is oscillating and it has not reached its maximum value. We observe that the weights have a sawtooth shape, which is due to changing phase in the downconverted output, which are not exactly at zero frequency, but very close to it. When we plot the error versus the number of samples, we can see that at first the error is quite sinusoidal, but as the adaptive filter learns to cancel the sinusoidal component, the error becomes increasingly random.

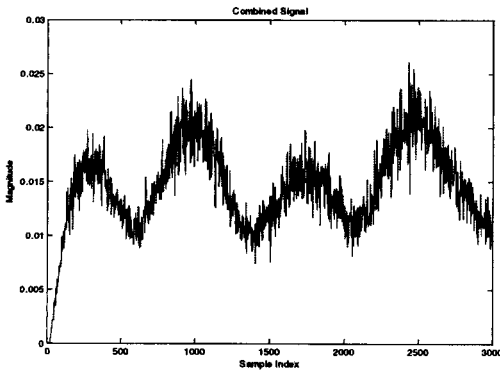


Figure 7. Combined output signal with  $\mu=10$ .

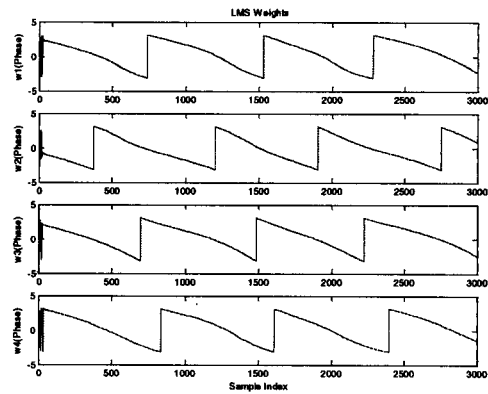


Figure 8. Phase of the weights with  $\mu=10$ .

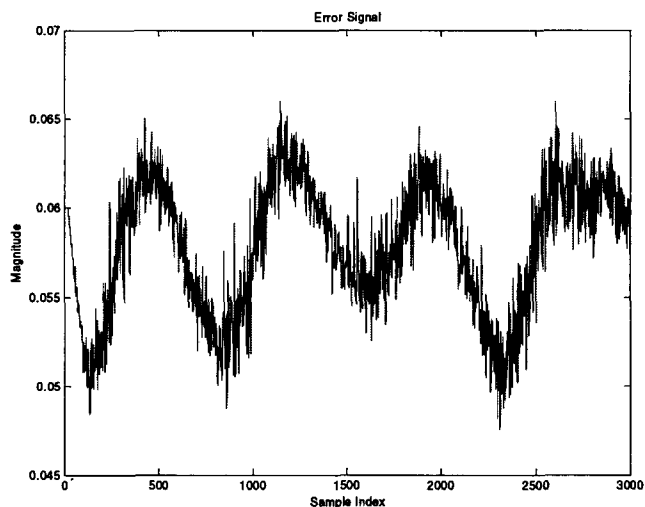


Figure 9. Error signal for  $\mu=10$ .

Regarding Figs. 10, 11 and 12, we observe that as we increase the value of the step-size, now with  $\mu=100$ , we get greatly improved performance. The combined output shown in Fig. 10 has increased in value approaching its maximum, which will be accomplished for even higher values of  $\mu$ . The error signal as we can see in Fig. 12 has drastically decreased showing the convergence of the weights.

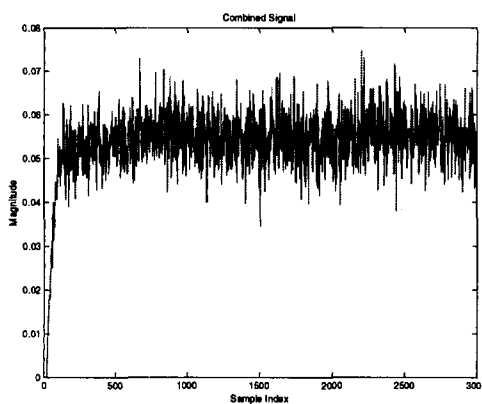


Figure 10. Combined output power with  $\mu=100$

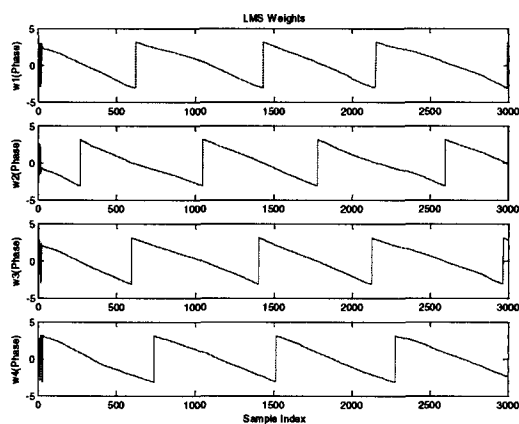
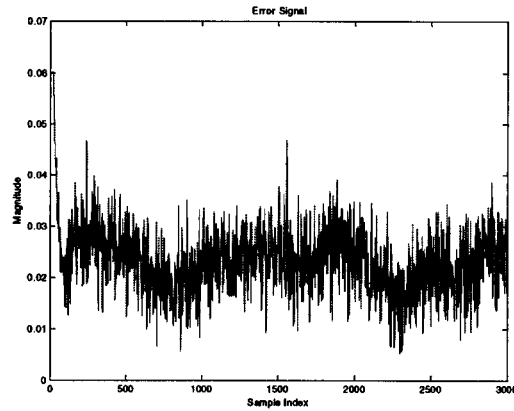
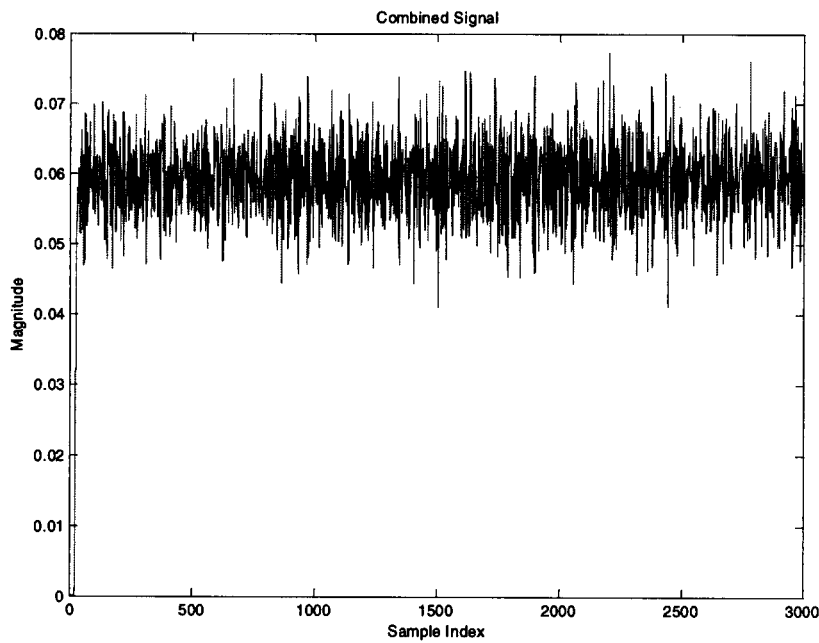


Figure 11. Phase of the weights with  $\mu=100$



**Figure 12.** Error signal with  $\mu=100$

Finally, when the stepsize is large enough so that the LMS algorithm is able to keep up with the phase-rotation of the complex downconverted beatnote, at  $\mu=1000$ , we see that the combined output signal reached its expected maximum value of 0.06 as we already calculated in advance as we explained earlier and that we used in Eq. (32) when applied to our algorithm code. With this optimum value of  $\mu$ , the error drops to zero and we can conclude that the signals are phased up.



**Figure 13.** Combined output signal with  $\mu=1000$

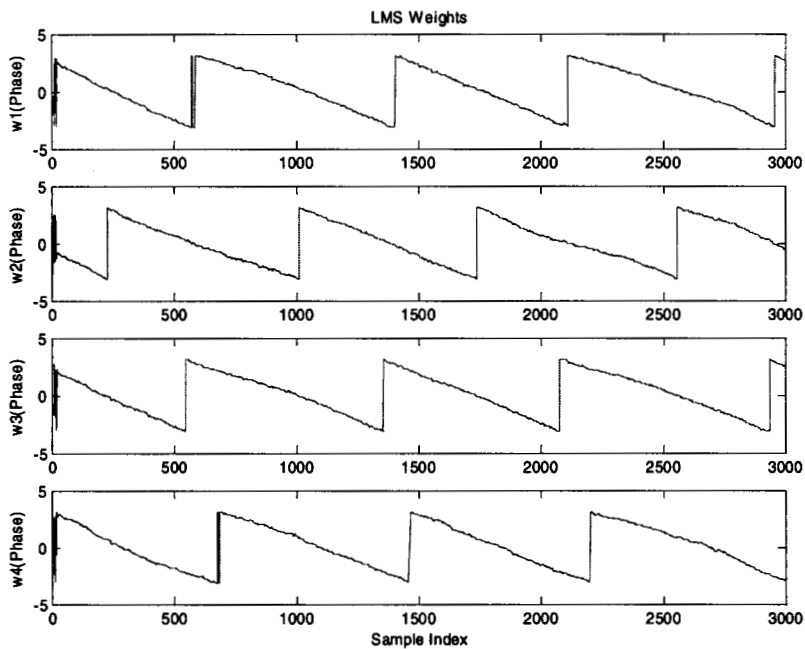


**Figure 14.** Phase of the weights of the four different channels with with  $\mu=1000$

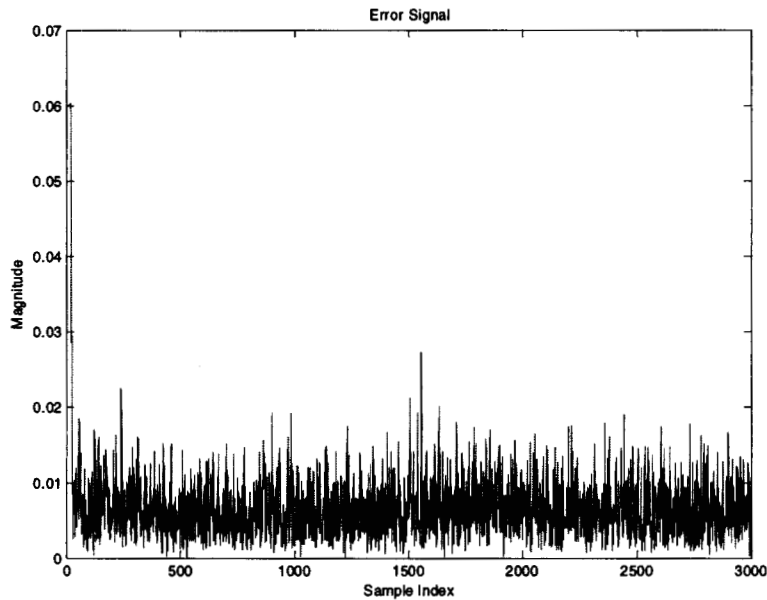


**Figure 15.** Error signal with  $\mu=1000$

These results illustrate as we expected, that increasing the step-size allows the LMS to be able to follow and track the phase-rotation of the complex downconverted beatnote and experimenting we found out that the optimum value of  $\mu$  for the particular case discussed here is 1000. For this value there is a perfect tracking of the phase of the weights and accordingly, the error signal drops to zero.

It is important to note that usually books and papers, the step-size is shown to be much smaller than one, but that is because the signal is assumed to be of unity amplitude. In our experiment, the signal level that we are dealing with is very small as there is not enough amplification after detection and as we mentioned earlier the signal is coupled to a detector and ac-coupled to eliminate the local oscillator signal.

#### 4. CONCLUSIONS AND FUTURE WORK

We have completed the laboratory setup for testing optical coherent communications using PPM modulation under simulated turbulence conditions. We have been able to track the phase of the beatnote signals coming out of the photodetector using the LMS algorithm producing an optimum signal combined output. We plan to modulate the signal with PPM in the future maintaining the pulse-to-pulse coherence of the optical fields (because of the external modulator) enabling the use of the LMS. It has to be mentioned too, that as we relax the requirements for inter-pulse coherence, there will be a need to use other combining algorithms that do not depend on temporal coherence on a short time-scale, using only the "geometrical" phases to combine the signal, such as suitably modified versions of a "constant modulus algorithm" (CMA) or other appropriate algorithms that we will develop to work also under turbulent conditions.

#### 5. ACKNOWLEDGMENTS

The authors would like to acknowledge Carlos Esproles for his help on the laboratory setup and Angel Portillo for his simulations contributions.

#### REFERENCES

1. R. M. Gagliardi, S. Karp, "Optical Communications," 2<sup>nd</sup> ed., Wiley Series in Telecommunications and Signal Processing, New York, 1995, Chapter 5.
2. M. Bass, (editor in chief), "Handbook of Optics, Fiber Optics and Nonlinear Optics," 2<sup>nd</sup> ed., Vol. IV, McGraw-Hill, New York, 2001, Chapter 1.
3. J. C. Palais, "Fiber Optic Communications," Prentice Hall, New Jersey, 1998, Chapter 10.
4. G. R. Osche, "Optical Detection Theory for Laser Applications," Wiley Series in Pure and Applied Optics, New Jersey, 2002, Chapter 1.
5. A. Yariv, "Optical Electronics," Holt, Rinehart and Winston, Inc., 1985, Chapter 11.
6. S. B. Alexander, "Optical Communication Receiver Design," The Society of Photo-Optical Instrumentation Engineers, 1997, Chapter 3.
7. C. N. Georghiadis, D. L. Snyder, "Receiver Performance for Heterodyne Optical Communication," IEEE Transactions on Communications, Vol. Com-34, No. 11, November 1986.
8. R. M. Gagliardi, S. Karp, "Optical Communications," 2<sup>nd</sup> ed., Wiley Series in Telecommunications and Signal Processing, New York, 1995, Chapter 6.
9. V.A. Vilnrotter, "An M-ary Coherent Optical Receiver for the Free-Space Channel," TDA Progress Report 42-66, Jet Propulsion Laboratory, Pasadena, September and October 1981.
10. J. M. Wozencraft, I. M. Jacobs, "Principles of Communication Engineering," John Wiley & Sons, Inc., New York, 1965, Chapter 4.
11. A. J. Viterbi, "Principles of Coherent Communications," McGraw-Hill Book Company, New York, 1966, Chapter 8.
12. v. A. Vilnrotter, M. Srinivasan, "Adaptive Detector Arrays for Optical Communications Receivers," IEEE Transactions on Communications, Vol. 50, No. 7, July 2002.
13. B. Widrow, S. D. Stearns, "Adaptive Signal Processing," Prentice-Hall Signal Processing Series, Prentice-Hall Inc., New Jersey, 1985, Chapter 6.
14. R.T. Compton, Jr., "Adaptive Antennas," Prentice-Hall Inc., New Jersey, 1988, Chapter 2.

\*[michela@caltech.edu](mailto:michela@caltech.edu), phone 1 818 354-9272; fax 1 818 393 1717; caltech.edu